Anal Bioanal Chem (2010) 396:2797–2804
DOI 10.1007/s00216-009-3120-2

ORIGINAL PAPER

Vacuum annealing phenomena in ultrathin TiD_y/Pd bi-layer films evaporated on Si(100) as studied by TEM and XPS

W. Lisowski · E. G. Keim

Received: 24 June 2009 / Revised: 25 August 2009 / Accepted: 29 August 2009 / Published online: 22 September 2009

Abstract Using a combination of TEM and XPS, we made an analysis of the complex high-temperature annealing effect on ultrathin titanium deuteride (TiD_y) films evaporated on a Si(100) substrate and covered by an ultrathin palladium layer. Both the preparation and annealing of the TiD_y/Pd bi-layer films were performed in situ under UHV conditions. It was found that the surface and bulk morphology of the bi-layer film as well as that of the Si substrate material undergo a microstructural and chemical conversion after annealing and annealing-induced deuterium evolution from the TiD_y phase. Energy-filtered TEM (EFTEM) mapping of cross-section images and argon ion sputter depth profiling XPS analysis revealed both a broad intermixing between the Ti and Pd layers and an extensive inter-diffusion of Si from the substrate into the film bulk area. Segregation of Ti at the Pd top layer surface was found to occur by means of angle-resolved XPS (ARXPS) and the EFTEM analyses. Selected area diffraction (SAD) and XPS provided evidence for the formation of a new $PdTi_2$ bimetallic phase within the top region of the annealed film. Moreover, these techniques allowed to detect the initial stages of TiSi phase formation within the film–substrate interlayer.

Keywords Palladium · Titanium deuteride · Silicon · TEM · XPS

W. Lisowski (✉)
Institute of Physical Chemistry, Polish Academy of Sciences,
Kasprzaka 44/52,
01-224 Warsaw, Poland
e-mail: wlis@ichf.edu.pl

E. G. Keim
MESA+ Research Institute, NanoLab, Materials Characterization,
University of Twente,
P.O. Box 217, 7500 AE Enschede, The Netherlands
e-mail: e.g.keim@utwente.nl

Introduction

Annealing studies of TiD_y/Pd bi-layer films are essential to improve the performance of Ti–H (Ti–D) compounds, well-known in the application of hydrogen storage media and in catalytic and energetic reactions [1, 2], or as material for the synthesis of fine-grained Ti-based alloys [3]. Evolution of hydrogen (deuterium) from such material is realized at elevated temperatures. The results of our recent studies related to titanium-deuterated films [4] and those reported by other authors [5, 6] revealed an essential role of the thickness dependent morphology of the Ti film towards the formation of a titanium deuteride (TiD_y) film and its subsequent decomposition. Annealing-induced decomposition of fine-grained thin TiD_y films of 10–20 nm thickness proceeds at much lower temperatures than the corresponding thicker films. The kinetics of this process was discussed in terms of an intermediate decomposition surface state towards the recombinative desorption of molecular deuterium [4]. In view of these results, we believe it would be interesting to investigate ultrathin TiD_y/Pd bi-layer films evaporated on quartz or Si substrate where both Ti–Pd interlayer diffusion and film–substrate interaction is expected to occur as a result of annealing processing. The results of our most recent studies related to ultrathin TiD_y/Pd films evaporated on quartz showed a progressive change in chemical composition within the surface and subsurface area of the film during annealing, leading to extensive inter-diffusion of Ti within the Pd top layer, strongly affecting the kinetics of deuterium desorption [7]. Si inter-diffusion from the quartz substrate layer could, however, not be observed. This observation stimulated our interest in the practical application of pure silicon as substrate for ultrathin TiD_y/Pd films. Silicon plates are used very often as material support for metal film deposition, and silicon/transition metal interfaces have been

intensively investigated since they enjoy wide application in highly miniaturized semiconductor devices [8].

In the present paper, we report the results of our experimental studies on the annealing of an ultrathin TiD_y/Pd film evaporated on a Si(100) substrate. We want to show how annealing-induced decomposition of titanium deuteride affects both the bulk and surface structure of an ultrathin TiD_y/Pd film, and what the tendency will be of the structural film as a result of annealing-induced film–silicon substrate interaction. In order to elucidate these points, we carried out a comparative investigation of Si/TiD_y/Pd films taken before and after annealing. The analysis of selected samples was performed using transmission electron microscopy (TEM)—in combination with energy-filtered TEM (EFTEM) and energy dispersive X-ray spectrometry (EDX), and X-ray photoelectron spectroscopy (XPS).

Experimental

Ultrathin Si/TiD_y/Pd film preparation was carried out following the same procedure as we used for the preparation of corresponding films on a quartz substrate [7]. Ten- to 20-nm-thick Ti films were evaporated within a glass UHV system [9] onto a Si(100) substrate plate kept within a glass preparation cell at 273 K at a pressure $\leq 1\times10^{-7}$ Pa. After evaporation, the films were annealed for 60 min at 650 K. The TiD_y films were then prepared by volumetrically controlled D_2 sorption at 298 K [10] until an equilibrium pressure of approx. 1 Pa was reached. After adsorption, deuterium was evacuated to the final steady pressure approaching 10^{-4} Pa, at which a 10–20-nm-thick Pd layer was evaporated.

Annealing of the Si/TiD_y/Pd film was performed in situ using the same procedure as we well established previously for TiD_y/Pd films evaporated on quartz [7]. The procedure was determined by the experimental conditions, in which decomposition of the deuteride phase was completed. Using a heating rate of 50 K/min decomposition of titanium deuteride was accomplished in 12–15 min in a temperature range 300–673 K [7]. Deuterium evolution as a result of annealing the TiD_y/Pd films was monitored in situ by mass spectrometry.

Morphological examination of the Si/TiD_y/Pd films before and after annealing was performed ex situ in separate analytical systems. Therefore, in order to compare the films before and after annealing, we prepared two separate Si/TiD_y/Pd film samples using the same preparation procedure. However, only one of these samples was annealed. In this way, we were able to prepare specimens representative of the Si/TiD_y/Pd films prior to annealing and the corresponding films after annealing processing, respectively.

TEM analyses were carried out in a Philips CM300ST-FEG, which was equipped with a Gatan Tridiem energy filter and Thermo Fisher Noran System Six EDX analyzer with nanotrace EDX detector. The TEM specimens of the analyzed films were prepared in cross-section (XS) according to the recipe described in Ref. [11]. XS-TEM images were used to extract information regarding the bulk structure of the corresponding films. Selected area diffraction (SAD) analysis allowed the crystal phases in the bulk of Si/Pd/TiD_y film to be identified. EFTEM analysis revealed the element distribution in both the bulk of films and Si substrate/film interface region. The three-window method was used for the EFTEM analysis in order to minimize interference from Pd and Ti. Verification of the correctness of the resulting Pd and Ti maps was provided by EDX analyses as well as EFTEM-spectrum imaging.

The characterization of the complex annealed TiD_y/Pd films has also been carried out using XPS. The XPS spectra were recorded in a PHI 5000 VersaProbe TM spectrometer using monochromatic Al-K_α radiation ($h\nu$=1,486.6 eV) from an X-ray source operating at 100 μm spotsize, 25 W and 15 kV. The analyzer pass energy was 23.5 eV and the energy step size was 0.1 eV. Both AR and argon-sputter profiling XPS analysis have been carried out. In the AR mode, the spectra were collected at electron take-off angles 10–90° relative to the surface plane. XPS sputter depth profiling was done using a 500-eV argon ion beam, a sputter area of 2×2 mm and a sputter rate of 1.4 nm/min, calibrated on a 100-nm-thick SiO_2 layer thermally grown on a Si substrate. The spectra were analyzed using the Casa XPS software. Shirley background subtraction and peak fitting with Gaussian–Lorentzian-shaped profiles was performed for all considered photoelectron peaks.

Results and discussion

Cross-sectional TEM analysis

Figure 1 shows the bright-field TEM (BFTEM) cross-sectional images of an ultrathin TiD_y/Pd film, recorded before (a) and after annealing-induced deuterium evolution (b). The TEM images are similar to those which we reported previously for thin TiD_y/Pd films evaporated on a quartz substrate [7]. We observed distinct, sharp, and well-separated areas of the TiD_y and Pd layers in the TiD_y/Pd film before annealing (a), and intermixed areas of Ti and Pd films forming an amorphous bulk structure morphology as a result of annealing processing (b). The morphology of the Si material in the area of the substrate close to the annealed film interface (b) seems to be significantly affected as well: irregular changes in Si bulk morphology are clearly visible within about 15 nm depth of the substrate. Shown below

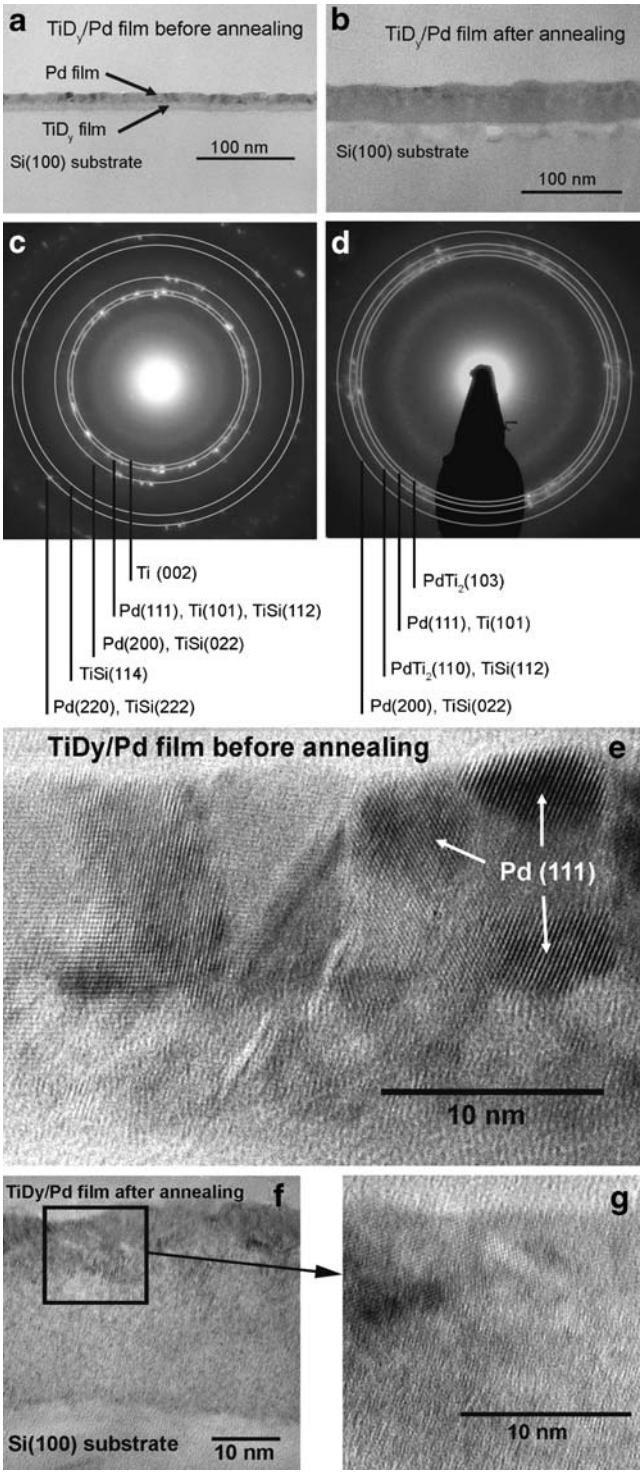

Fig. 1 Low-magnification TEM cross-sectional bright-field images (BFTEM) of the TiD_y/Pd films evaporated on Si(100) taken before (**a**) and after (**b**) annealing. The SAD patterns recorded on the corresponding films before and after annealing are shown in images **c** and **d**, respectively, together with the assignment of the most relevant low-index Miller planes of the diffraction spots. Below are shown the high-magnification cross-sectional TEM lattice images of the Si/TiD_y/Pd top layer before (**e**) and after annealing (**f**, **g**). The Pd grains with a dominant (111) orientation are marked in (**e**)

the BFTEM images are the corresponding SAD patterns ((c) and (d) for the Si/TiD_y/Pd film before and after annealing, respectively) from which certain crystallographic properties can be retrieved. From a direct measurement of the radius between the central spot and the diffraction spots lying on artificial concentric circles (in Fig. 1c and d shown as semitransparent gray circles drawn through the relevant diffraction spots), the Miller index planes could be determined. From the diffraction pattern describing the Si/TiD_y/Pd film prior to deuterium evolution (c) the most relevant crystallographic planes belonging to the Pd fcc structure could be identified (mainly Pd (111), and in addition Pd (200) and Pd (220)). A small contribution of Ti hcp and TiSi structures should also be considered although their identification is difficult because most of the crystallographic planes belonging to Ti (Ti (101)) and TiSi (TiSi (112), TiSi (022), and TiSi (222)) overlap with the crystallographic planes of Pd [12]. No distinct diffraction spots associated with the TiD_2 crystalline form were observed. The diffraction pattern of the film after annealing (d) disclosed very weak and diffuse diffraction spots, which can be assigned to coexisting Pd fcc, Ti hcp, $PdTi_2$, and TiSi [12] crystallographic phases. However, the low-intensity spots in the diffraction pattern seem to indicate that the contribution of crystalline phases in the annealed film is very small. Supporting evidence is provided by the high-magnification cross-sectional TEM lattice images presented in Fig. 1e, f, and g: very fine polycrystalline grains (6–8 nm), originated mainly from the Pd phase in (e), are consistent with the weak diffraction spots in Fig. 1c, whereas the dominant amorphous areas in addition to the rare polycrystalline grains in the annealed film (f, g) can explain the observed weak and diffuse diffraction pattern presented in (d).

In Fig. 2, the results of the EFTEM analyses on the cross-section planes of the TiD_y/Pd film taken before (left column) and after (right column) annealing-induced deuterium evolution are presented. In these columns, the BFTEM images, together with the associated EFTEM elemental mappings of Si ($L_{2,3}$ edge), Ti ($L_{2,3}$ edge), and Pd ($M_{4,5}$ edge), are compared. The elemental distribution is marked in white color (an area with bright intensity represents a higher elemental concentration than an area with dark intensity). To visualize the elemental distribution even more clearly, the elemental maps are combined into an RGB composite image presented in the far right column of Fig. 2. In this figure, each elemental map of Si, Ti, and Pd is associated with a color, i.e., blue, green, and red, respectively.

The EFTEM images reveal that as a result of the annealing, an extensive intermixing process between the Ti and Pd layers occurs as well as a significant Si and Ti inter-diffusion within the Ti film and Si substrate region, respectively. Silicon is not detected on the top of annealed

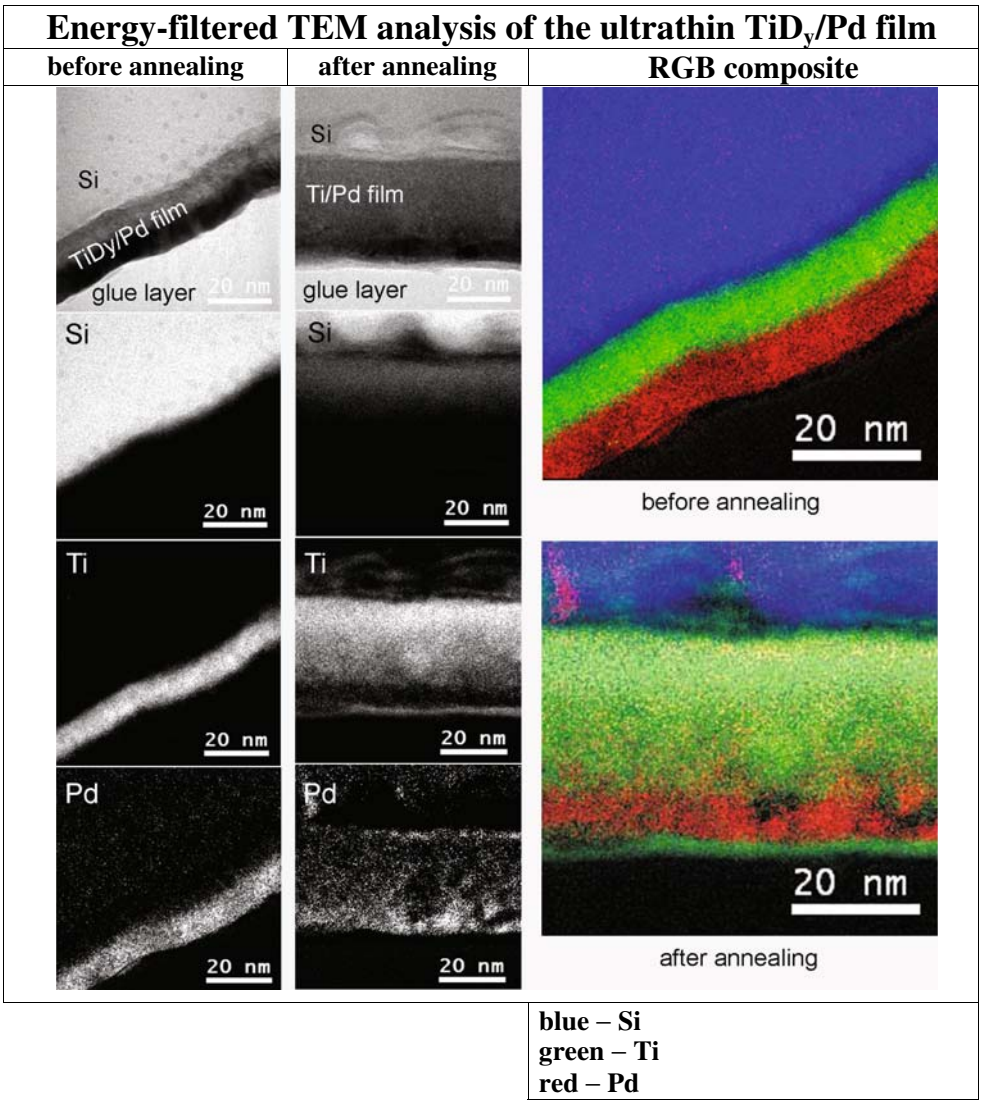

Fig. 2 EFTEM analysis of the Si/TiD$_y$/Pd layer before (*left column*) and after annealing processing (*right column*). The bright-field TEM (BFTEM) cross-sectional images of both films are presented on top of each column. Below the BFTEM images are shown the associated elemental mappings of Si ($L_{2,3}$ edge), Ti ($L_{2,3}$ edge), and Pd ($M_{4,5}$ edge). The elemental distribution is marked in *white color*. On the far right, the RGB images of the ultrathin Si/TiD$_y$/Pd film taken before and after annealing are shown, as created by superimposing the elemental EFTEM maps of Si (*blue*), Ti (*green*), and Pd (*red*)

film but the depth of Si atom penetration within the Ti/Pd interlayer is roughly more than 15 nm as estimated from the EFTEM mapping images. One can also observe a visible enrichment of Ti on the top surface of the Pd film.

XPS analysis

The chemical nature of the components formed within the surface and subsurface areas as well as in the bulk region of the annealed TiD$_y$/Pd films was investigated using XPS. The bulk distribution of elements within the films, taken before and after annealing, were analyzed by means of ARXPS and XPS ion argon-sputter depth profile analyses.

XPS surface and subsurface analysis

Figure 3 shows the XPS survey spectra obtained before (spectrum 1) and after (spectrum 2) annealing-induced deuterium evolution from the Pd/TiD$_y$ film. The presence of Ti peaks, in addition to those associated with Pd, can be clearly observed in spectrum 2. Silicon peaks were not detected in the surface region of both films.

The relative distribution of Ti and Pd within the surface and subsurface region of the annealed film was revealed by the ARXPS spectra, of which the analysis results are presented in Fig. 4. This was done by measuring the areas of all detail photoelectron peaks of Pd 3*d* (a) and Ti 2*p* (b), recorded on the annealed film collected at electron take-off angles in the range of 10–90°. As a result, the relative atomic concentration ratio Ti 2*p*/Pd 3*d* at various depths within the surface and subsurface regions of the film was derived (c). The result of this analysis disclosed a significant enrichment of Ti on the top Pd layer. The chemical nature of Ti compounds at the top-most section of the film surface area can be determined from an analysis of the ARXPS spectra of Ti 2*p* in Fig. 4b, where at low angles (10° and 20°), only TiO_2

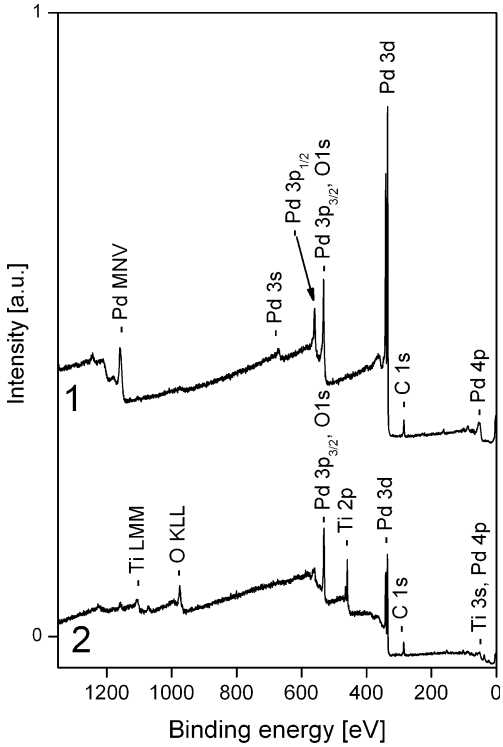

Fig. 3 Wide XPS binding energy spectra of the Si/TiD_y/Pd film surface taken before (*line 1*) and after (*line 2*) annealing processing. Both XPS spectra were recorded after removing about 1.4 nm of the Pd top layer by Ar^+ sputtering

peaks could be detected (see Ti $2p_{3/2}$ peak at 458.6 eV, and its corresponding Ti $2p_{1/2}$ peak at 464.2 eV BE).

In order to analyze the chemical nature of Pd compounds and their relative depth distribution within the surface/subsurface interface, we estimated that the areas of all peaks result from a deconvolution of the Pd 3*d* XPS spectra. The analysis of this spectrum (Fig. 5a) reveals the coexistence of three doublets in the Pd 3*d* spectra (Pd $3d_{5/2}$ peaks positioned at 335.0, 336.0, and 337.9 eV BE, and its corresponding Pd $3d_{3/2}$ peaks at 340.3, 341.6, and 343.2 eV BE, respectively), which can be ascribed to Pd, $PdTi_2$, and PdO_2 [13]. In Fig. 5b, a relative atomic concentration depth-contribution of the detected Pd compounds within the surface–subsurface region is shown. One can see that the Pd atom concentration is relatively higher on the top film surface area than in the film subsurface and bulk region (see the low-angle XPS data). In deeper bulk film areas, the relative concentration of the $PdTi_2$ becomes even higher than Pd (see later), which indicates that the Ti, of which the segregation was detected on the top of the Pd layer, does not only originate from the $PdTi_2$ but also from the bottom TiD_y layer forming apparently titanium oxides. This conclusion supports very well the results of the ARXPS Ti 2*p* measurements (Fig. 4b) presented above.

XPS depth-profiling analysis

Both Si/TiD_y/Pd samples, taken prior to and after annealing were depth-profiled using XPS analysis to reveal the Pd, Ti, and Si bulk distribution within both films. Because both films were prepared and analyzed under the same experimental conditions, we assume that all sputter-profiling-induced effects, as discussed in Ref. [14], are similar for these films. Therefore, in spite of thickness differences between the two films investigated, in a direct comparison of the elemental depth profiles, these sputter-profiling-induced artifacts are canceled out, thus disclosing only the difference in the Pd, Ti, and Si distribution in the films caused by the annealing and annealing-induced deuterium evolution processes.

Figure 6 shows the XPS depth profiles of both compared films. The depth distribution of palladium, titanium, silicon, and carbon evaluated from the Pd 3*d*, Ti 2*p*, Si 2*p*, and C 1*s* XPS peaks, respectively, is shown as a function of sputter time. The analysis of the oxygen depth distribution in the samples investigated was rather doubtful because of the overlap of the O 1*s* and Pd $3p_{3/2}$ states. However, the oxygen

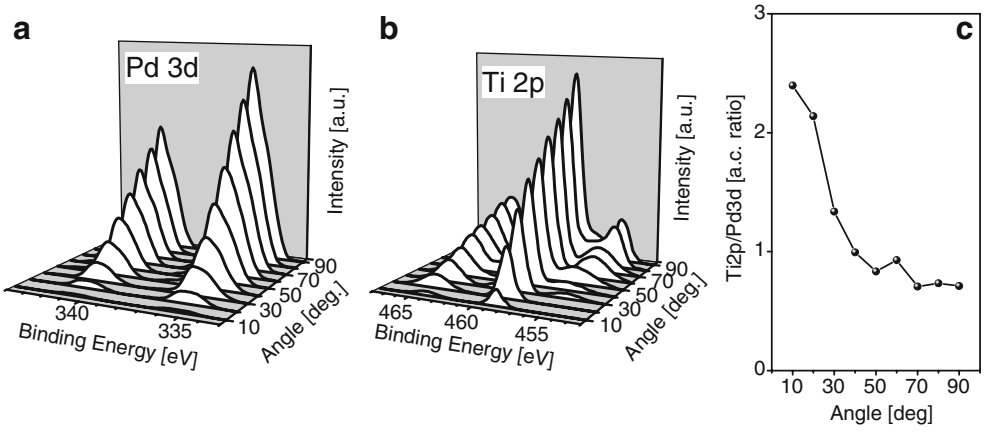

Fig. 4 Analysis of the Pd 3*d* (**a**) and Ti 2*p* (**b**) angle-resolved ARXPS spectra collected at angles in the range of 10–90° on the Si/TiD_y/Pd layer after annealing: the relative atomic concentration ratio of Ti 2*p*/Pd 3*d* at various depths of the surface and subsurface regions of the annealed film is shown in (**c**)

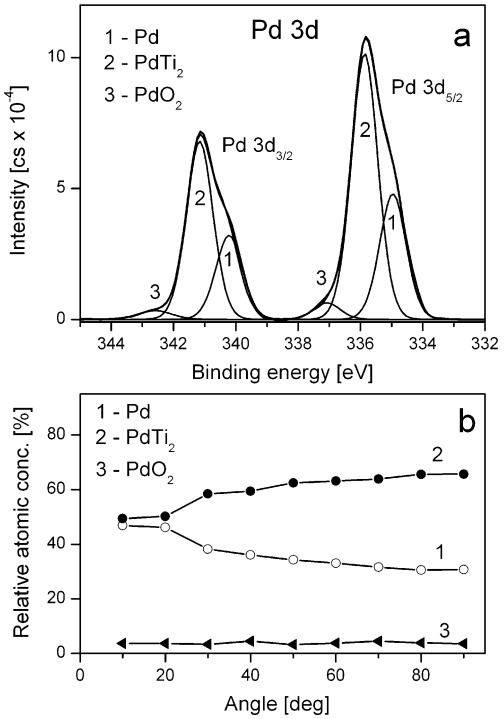

Fig. 5 **a** The peak-fit analysis of the Pd 3*d* XPS spectrum, taken at 90° on the annealed Si/TiD_y/Pd layer surface. **b** Analysis of the angle-resolved ARXPS spectra of the Pd 3*d* region. The relative atomic concentration of the Pd compounds (marked in **a**) within the surface–subsurface region of the annealed film was estimated from the Pd 3*d* XPS spectra collected at angles in the range of 10–90°

distribution in the film–Si substrate interface region could be derived by monitoring the depth profile of SiO_2, i.e., by measuring the Si 2*p* signal. Both samples were pre-sputtered for 1 min in order to remove the carbon surface contamination (in this time, approx. 1.4 nm surface contamination was removed).

The elemental depth profiles for the sample prior to annealing, presented in Fig. 6a, revealed the Pd to be the sole component in the initial stage of depth profiling. At larger depths, the change from the Pd to TiD_y layer and then to the Si substrate appear to proceed in a gradual fashion. The partially overlapping elemental profiles reveal an intermixing zone, which is expected to be the result of preferential ion-sputtering effects [14, 15]. More complex intermixed changes can be observed within the TiD_y–Si substrate interface region where minor contamination by silicon oxide and silicon carbide was detected. The Si 2*p* XPS spectra recorded in depth of the Ti–Si mixed region were found to be shifted to 99.2 eV BE, lower than we determined on the pure Si substrate (99.4 eV), indicating a partial interaction of the Si substrate with evaporated Ti film leading to the formation of titanium silicide [16–18]. However, we did not observe any extensive inter-diffusion of Si through the entire set of TiD_y–Pd layers.

Short-time annealing at 673 K, implicating deuterium evolution from the TiD_y phase, causes substantial reaction and intermixing of Ti, Pd, and Si across the initial Pd/TiD_y and TiD_y/Si interfaces, as shown in Fig. 6b. As a result, the profiles for Pd, Ti, and Si are considerably broader than observed for samples prior to annealing (Fig. 6a). We observe very extensive inter-diffusion of Ti through the Pd layer and segregation towards the top Pd surface, as well as interaction of Ti with interdiffusing Si from the substrate material. Relatively broad profiles of C 1*s* and SiO_2 were recorded within the Ti–Si interface region. However, in this case, in contrast with the unannealed film, where the C 1*s* spectra originated only from silicon carbide, the C 1*s* spectra reveal both the aliphatic carbon and silicon carbide.

From the elemental XPS spectra, recorded after the following discrete steps during depth profiling, various chemical compounds formed at various depths of the annealed film could be identified. As an example, in Fig. 7, we present the result of an analysis of the Si 2*p* profile. The chemical nature of these spectra is illustrated in Fig. 7a, in which also a Si 2*p* spectrum is shown, which was recorded in a separate experiment from pure substrate material (spectrum (e)). One can see that all Si 2*p* spectra, recorded in the depth profiling of the annealed sample, are

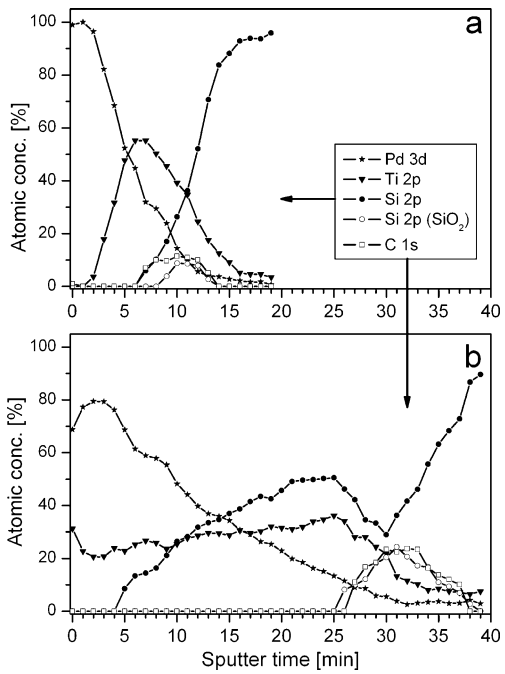

Fig. 6 XPS sputter depth profiles of the Si/TiD_y/Pd layers taken before (**a**) and after (**b**) annealing. The relative atomic concentration depth distribution of palladium, titanium, silicon, and carbon evaluated from the Pd 3*d*, Ti 2*p*, Si 2*p*, and C 1*s* XPS peaks, respectively, are shown as a function of sputter time (sputter rate: 1.4 nm/min relative to a 100-nm-thick SiO_2/Si layer). The selected Si 2*p* XPS profile of SiO_2 is also shown for better characterization of the contaminants in the film–substrate interface area

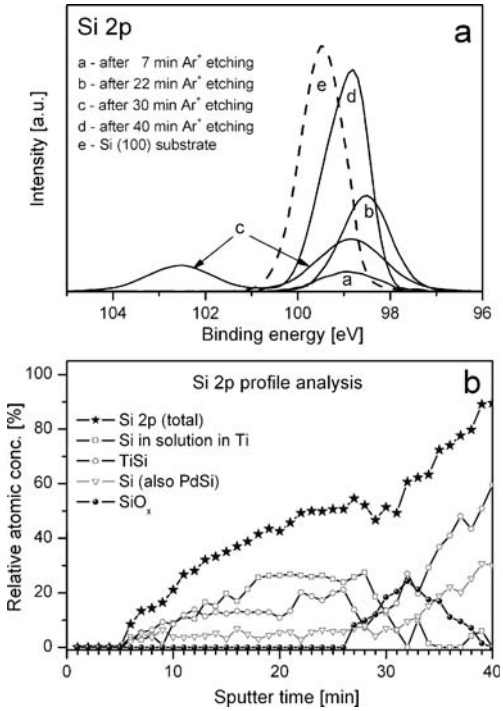

Fig. 7 **a** The Si 2*p* XPS spectra taken after subsequent steps of Ar^+ sputtering (see lines marked as *a*, *b*, *c*, and *d*). The Si2p spectrum (*e*) was recorded separately from pure Si(100) substrate material. **b** The analysis of the Si 2*p* XPS sputter depth profile of the annealed Si/TiD_y/Pd layer. For a detailed description, see the text

shifted towards lower BE values as compared with the pure Si material, an indication that titanium silicide is the dominant intermetallic compound in the whole analyzed depth area of the film. The relatively high shift in BE (−0.6 to −0.9 eV) is more likely to be associated with TiSi (−0.6 eV [17]) than with $TiSi_2$ (−0.2 eV [18]). Therefore, for the analysis of the Si 2*p* depth profile, we used the BE value of our pure reference Si substrate (99.4 eV) correlated with BE values found by other authors for TiSi (BE shift −0.6 eV [17]) and Si in solution in Ti (BE shift −1.1 eV [17]): The coexistence of silicon oxides and palladium silicides was also analyzed although the Si 2*p* peak in PdSi shows significant overlap with that in Si (Si 2*p* BE 99.5 eV [19] and 99.4 eV [16], respectively). As shown in Fig. 7b, TiSi and interdiffused Si are major components within the annealed film. On the other hand, titanium silicide is also a dominant intermetallic component found in the top of the substrate layer. This result is in agreement with the EFTEM images reflecting heavy Ti inter-diffusion within both the Pd film and Si substrate phases. Silicon oxide has only been observed within the film–substrate interface.

Discussion of annealing processes

The experimental data presented above shows the effects of two various/subsequent annealing procedures applied in the Si/TiD_y/Pd film processing. The first annealing procedure was carried out routinely for both compared samples as part of one of the stages of the Ti film preparation prior to deuterium sorption. The aim of this annealing stage was to remove all absorbed gasses (mainly nitrogen) from the Ti film, which could affect the subsequent deuterium sorption. In our case, the effects of this annealing processing step can be analyzed in the "as prepared" Si/TiD_y/Pd film. Taking into account the time and temperature of this annealing step (60 min, 650 K), an initial Ti–Si reaction is expected to occur leading to the observed TiSi and $TiSi_2$ phase formation. Similar low-temperature (approx. 570 K) initial reactions at the Ti–Si interface has been reported by other authors [15, 17]. Both the SAD patterns presented in Chapter 3.1 (Fig. 1 c and d) and the Si 2*p* XPS spectra provided evidence for the coexistence of a titanium silicide phase in the "as prepared" Si/TiD_y/Pd film. However, sharp boundaries between the PdD_y, Ti, and Si phases in the EFTEM images (Fig. 2) indicate that there is no significant amount of inter-diffusion of Si. It is likely that inter-diffusion of Si into Ti is partially retarded by SiO_2 and SiC species [20], whose small contamination level has been detected in the film–substrate interface (see XPS depth profiles in Fig. 6a).

The second annealing procedure we used for the finally prepared Si/TiD_y/Pd film in order to evolve deuterium from the TiD_y phase. This process was completed in 12–15 min in the temperature range 300–675 K using a heating rate of 50 K/min. In spite of the fact that the final annealing temperature was only 25 K higher than used for the preliminary Ti/Si film annealing, and the associated time of annealing being much shorter, we observed a substantial structural and chemical rearrangement of the film. Both EFTEM images and XPS sputter profiles provided evidence for an extensive inter-diffusion of Ti, Pd, and Si. Similar annealing-induced inter-diffusion phenomena of Ti and Pd have been reported previously for thin TiD_y/Pd films prepared on quartz [7]. However, we did not find any evidence for serious inter-diffusion effects of Si from the quartz substrate layer. In contrast, the annealing of the ultrathin TiD_y/Pd films prepared on a Si(100) substrate induced an extensive interaction of Si with these films.

This work shows that interaction with deuterium atoms, released during annealing, induces various processes leading to a chemical and structural transformation of the Si material within the film–substrate interface and accelerating reactive inter-diffusion of Si and Ti. Hydrogen (deuterium) interaction with Si has been the subject of active research reported well in literature (see, e.g., Ref. [21]). Low-temperature hydrogen interaction with pure Si material was found to form SiH_x species, which decomposes at temperatures higher than 670 K [21, 22]. However in our films, this ideal scheme of deuterium–silicon interaction should be considered as just

one of various processes proceeding simultaneously in the TiD_y–Si interface. Indeed, deuterium released from the TiD_y phase can interact with the Si substrate interface forming Si–D species and initialize interaction of pure Ti decomposed from the TiD_y phase with Si. This simple mechanism is however, complicated by SiO_2 and TiO_x interface contaminants and also by the structural phase transformation effects like amorphization or stress. The formation of amorphous material is usually observed as an intermediate state of crystal phase transformation. This tendency is well supported by the BFTEM cross-section and SAD images of the annealed film (see Fig. 1). Stress accompanying the structural phase transformation was considered by other authors [23] as a source of the very early stages of the Ti–Si reaction and $TiSi_2$ phase growth. On the other hand, tensile stress can induce deformation of the film and its separation from the substrate. We observed these two phenomena on our annealed samples. The BFTEM images reveal a visible amorphous Ti–Si interlayer (see Fig. 1), EFTEM shows extensive penetration of Ti within the Si (Fig. 2) and XPS depth profile analysis discloses much higher concentrations of SiC, TiO_2, and SiO_2 compared with the "as prepared" sample (Fig. 6). These observations, as well as the detection of aliphatic carbon in the interface region indicate a partial detachment of the film–substrate interlayer as a result of annealing.

Summary and conclusions

Structural and chemical phenomena accompanying the annealing of ultrathin TiD_y/Pd films evaporated on a Si (100) substrate have been investigated. It was found that the short annealing time at 673 K, inducing deuterium evolution from the TiD_y phase, causes substantial reactions and intermixing of Ti, Pd, and Si across the initial Pd/TiD_y and TiD_y/Si interfaces. The surface and bulk morphology of the bi-layer film as well as the Si substrate material undergo microstructural and chemical conversions. Broad intermixing between the Ti and Pd layers and an extensive interdiffusion of Si and Ti within the film–substrate interlayer have been observed as evidenced by energy-filtered TEM and XPS argon ion sputter depth profiling. The cross-section TEM images reveal a dominant contribution of the amorphized material in the annealed film. However, SAD pattern analysis revealed also the presence of very fine crystallites of $PdTi_2$ and an indication of the formation of a TiSi phase in the initial stages. Evidence for segregation of Ti towards the Pd top layer surface was provided by angle-resolved XPS and EFTEM.

References

1. Westlake DG, Satterthwaite CB, Weaver JH (1978) Phys Today 31:32–39
2. Hirooka Y (1984) J Vac Sci Technol A 2:16–21
3. Moon KI, Lee KS (1998) J Alloys Compd 264:258–266
4. Lisowski W, Keim EG, Kaszkur Z, Smithers MA (2008) Appl Surf Sci 254:2629–2637
5. Nowicka E, Duś R (1996) Langmuir 12:1520–1527
6. Checchetto R, Gratton LM, Miotello A, Tomasi A, Scardi P (1998) Phys Rev B 58:4130–4137
7. Lisowski W, Keim EG (2009) Anal Bioanal Chem 393:1923–1929
8. Murarka SP(1995) Intermetallics 3: 173–186
9. Lisowski W (1999) Vacuum 54:13–18
10. Duś R, Lisowski W, Nowicka E, Wolfram Z (1995) Surf Sci 322:285–292
11. Lisowski W, Keim EG, Smithers M (2002) Appl Surf Sci 189:148–156
12. Powder Diffraction File, Joint Committee on Powder Diffraction Standards, ICDD, 1999, Pd: card 46-1043, Ti: card 44-1294, $PdTi_2$: card 18-0957, TiSi: card 72-2115
13. Bzowski A, Sham TK (1993) Phys Rev B 48:7836–7840
14. Briggs D Grant JT(2003) (eds) Surface Analysis by Auger and X-ray Photoelectron Spectroscopy, IM, Chichester UK
15. Butz R, Rubloff GW, Tan TY, Ho PS (1984) Phys Rev 30:5421–5429
16. Wagner CD, Naumkin AV, Kraut-Vass A, Allison JW, Powell CJ, Rumble JR Jr (2003) NIST Standard Reference Database 20, Version 3.4, Web Version: http://srdata.nist.gov/xps/
17. Chambers SA, Hill DM, Xu F, Weaver JH (1987) Phys Rev B 35:634–640
18. Lee SM, Ada ET, Lee H, Kulik J, Rabalais JW (2000) Surf Sci 453:159–170
19. Dai DX, Davoli I (1995) Vacuum 46:139–142
20. Berti M, Drigo AV, Cohen C, Siejka J, Bentini GG, Nipoti R, Guerri S (1984) J Appl Phys 55:3558–3565
21. Oura K, Lifshits VG, Saranin AA, Zotov AV, Katayama M (1999) Surf Sci Rep 35:1–69
22. Kulkarni SK, Gates SM, Greenlief CM, Sawin HH (1990) Surf Sci 239:26–35
23. Bentini GG, Nipoti R, Armigliato A, Berti M, Drigo AV, Cohen C (1985) J Appl Phys 57:270–275